Asia-Pacific Journal of Atmospheric Sciences
https://doi.org/10.1007/s13143-024-00365-5

Online ISSN 1976-7951
Print ISSN 1976-7633

S.I. : ABNORMAL CLIMATE IN 2022 SUMMER IN KOREA AND ASIA

The Predictability of a Heavy Rainfall Event during the Summer of 2022 Using an All-sky Radiance Assimilation Experiment

Hyo-Jong Song[1] · **Sihye Lee**[2]

Received: 1 February 2024 / Revised: 18 April 2024 / Accepted: 19 April 2024

Abstract
This paper presents the results of the recent development of the all-sky radiance assimilation system in the Korean Integrated Model (KIM). In the cycled analysis and forecast experiments, the increased coverage of radiance data in cloudy regions improved the quality of initial fields for mass variables, temperature and humidity. The experimental period covered the record-breaking heavy rainfall event on August 9, 2022. We examined the simulation accuracy of the western North Pacific subtropical high (WNPSH) in both clear- and all-sky experiments. In the clear-sky experiment, northward propagation of the WNPSH was restricted. A humid bias exists with clear-sky radiance assimilation over the WNPSH region. Since humid air is lighter than dry air, in this situation, the geopotential height (GPH) should be lower to achieve the same pressure, and a low-pressure bias occurs. All-sky radiance assimilation dries the moisture field, which helps elevate the GPH over the WNPSH region. The expansion of the WNPSH yielded a steeper confrontation in the air between the land and ocean around the southeastern sea of the Korean Peninsula to predict the strength of rainfall events more accurately. A more accurate simulation of the jet stream outlet was also demonstrated in an all-sky experiment. This study shows that the all-sky radiance assimilation can help to more accurately predict extreme rainfall events via proper simulations of large-scale fields.

Keywords All-sky radiance · heavy rainfall · data assimilation · initial condition · KIM

1 Introduction

In the summer of 2022, torrential rainfall events occurred across the Korea Peninsula. On August 8−9, 2022, it rained explosively in the Seoul metropolitan area within a short time period. Owing to the narrow width of the precipitation system, many places were excluded from the effects of such explosive precipitation, even within the Korean Peninsula. Concentrated precipitation in such a narrow convection band is thought to have a different mechanism behind the wider monsoonal rainfall events. Numerical prediction models were used to identify the precipitation mechanisms. In particular, attempts have been made to identify differences in precipitation simulation results according to differences in initial conditions, and to indirectly reveal latent mechanisms in the precipitation system through this (Argence et al. 2008; Khadke and Pattnaik 2021).

All-sky microwave radiances that are sensitive to water vapor, clouds, and precipitation contribute around 20% of the observational impact on the short-range forecasting skill at the European Center for Medium-range Weather Forecasts (ECMWF) (Geer et al. 2017). Even ignoring the cloud and precipitation information, it would be beneficial to obtain more information on temperature and moisture (and indirectly, wind) in situations where the radiances are sensitive to a combination of temperature, water vapor, and hydrometeors (i.e., liquid or frozen water particles) (Geer et al. 2018). Better initialization of the mass and wind fields can lead to improved forecasts in the medium range. For example, the intensity of frontal precipitation can be brought closer to the observations by adjusting the strength of an associated low-pressure system (Geer et al. 2014). It is well known that the amount of water supplied affects the precipitation system (Khadke and Pattnaik 2021). Differences in initial moisture conditions occur according to the assimilation of clear-sky radiance or all-sky radiation (Lee et al. 2020). Based on these two facts, we directly generated initial moisture

✉ Sihye Lee
shlee@kiaps.org

[1] Department of Environmental Engineering and Energy, Myongji University, Yongin-si, Gyeonggi-do, South Korea

[2] Korea Institute of Atmospheric Prediction Systems, 35, Boramae-ro 5-gil, Dongjak-gu, Seoul, South Korea

Published online: 29 April 2024

conditions that were produced differently according to the assimilation of clear-sky and all-sky radiance and examined their effects on the prediction of precipitation systems.

This paper presents the results of the recent development of the all-sky radiance assimilation system in the Korean Integrated Model (KIM). The assimilation of the observation of a specific variable affects the quality of the initial conditions of other variables (Lee and Song 2018), particularly because moisture affects geopotential height (GPH). After a certain number of forecasting and data assimilation cycles, of which period covered the record-breaking heavy rainfall event on August 9, 2022, have been performed, there is a difference in the initial conditions of the GPH. The impact of all-sky radiance assimilation in the summer precipitation event, through the change in GPH of the initial conditions, is studied.

In Section 2, the experimental designs for clear-sky and all-sky radiance assimilation are presented, and their differences are identified. In Section 3, the differences between the predicted results of each experiment are identified and linked to the differences in the initial conditions. Section 4 draws tentative conclusions from these results regarding precipitation events.

2 Method

2.1 KIM and a Hybrid-4DEnVar System

The Korean Integrated Model (KIM), an operational non-hydrostatic global atmospheric model, uses the spectral element method on a cubed-sphere grid structure (Choi and Hong 2016; Hong et al. 2018). The KIM physics package includes a revised radiation scheme based on the rapid radiative transfer model for Global Circulation Models (Baek 2017), the revised Noah land surface model (Koo et al. 2017), a scale-aware nonlocal planetary boundary layer (Lee et al. 2018), and sub-grid orographic gravity wave drag (Choi and Hong 2015). In particular, the KIM uses scale-aware mass-flux deep convection (Kwon and Hong 2017) and shallow convection (Han et al. 2016), cloud microphysics based on the Weather Research Forecasting (WRF) single-moment 5-class (WSM5; Hong et al. 2004) including the effective radius for hydrometeors (Bae et al. 2016), and the prognostic cloud fraction scheme developed by Park et al. (2016).

The KIM with 91 vertical levels (the highest level at 0.01 hPa) contains a hybrid four-dimensional ensemble variational assimilation (Hybrid-4DEnVar) system. The horizontal resolutions are 50 km (operationally 32 km) for the Hybrid-4DEnVar, and 25 km (operationally 12 km) for the KIM background. In Hybrid-4DEnVar, a 6-hour analysis window is used, and the ensemble trajectory is represented with seven hourly times. A 50-member ensemble of 50 km resolution is initialized with a local ensemble transform Kalman filter (LETKF; Shin et al. 2018). The ratio of ensemble background error covariance varies, such as 0.7 near Tropics and 0.3 near the poles with smoothly transition. The static control variable incorporates a wind-mass transformation based on temperature-wind regression (Song et al. 2017). The analyses consist of increments to the horizontal wind components, potential temperature, density, mixing ratio, and dry surface pressure, with the latter derived via a hydrostatic balance equation during a post-processing step (Kwon et al. 2018). Only the central analysis increment is added to the KIM using an Incremental Analysis Update (IAU) method with a triangular time-weighting function whose apex is centered on the increment's validity time (Bloom et al. 1996; Lee et al. 2022).

2.2 Data Assimilation Experiments

To investigate the impact of cloud-affected radiance assimilation, we assimilated operational KIM observations (Kang et al. 2018) from a company with all-sky microwave satellite sensors during the period from 0000 UTC on 7 July 2022 to 1800 UTC on 15 August 2022. In particular, July to August 2022 is a period to analyze the precipitation forecast performance of the KIM due to frequent precipitation. In this study, all-sky radiances for Microwave Humidity Sounder (MHS) channels 3 ~ 5 and Advanced Technology Microwave Sounder (ATMS) channels 18 ~ 22 were assimilated. RTTOV-SCATT version 13.0 has been used as the observation operator, which provides multiple scattering radiative transfer calculations at microwave frequencies (Bauer et al. 2006). We used individual hydrometeors (e.g., cloud water, cloud ice, rain, and snow) for the radiation scheme of RTTOV-SCATT, and bulk optical properties were derived from a range of particle models, including Mie spheres (liquid and frozen) and nonspherical ice habits from the Atmospheric Radiative Transfer Simulator (ARTS) databases (Eriksson et al. 2018; Geer et al. 2021).

Bias correction (BC) for cloudy observations has been performed using BC coefficients calculated from clear-sky pixels because there are no significant benefits in the various attempts at cloud-related BC schemes (Geer et al. 2018; Okamoto et al. 2018). In the quality check, the threshold for outlier rejection was determined by the symmetric cloud amount, which was adopted by the averaged scattering index (Eqs. (1) and (2) of Lee et al. 2020). The observation errors for all-sky MHS/ATMS radiances were based on a symmetric observation error model suggested by Geer and Bauer (2011) and were estimated with standard deviations of first-guess departures as a function of the symmetric cloud amount. The observation errors for clear-sky MHS/ATMS radiance

Table 1 Comparison of the experimental settings between the current work and Lee et al. (2020)

Components	Lee et al. (2020)	Current work
Model	KIM v3.3 (resolution: 25 km, 0.01 hPa)	KIM v3.8 (resolution: same as Lee et al. (2020))
Data assimilation	Single loop (w/o update the background state)	Multiple outer-loop (update the background state)
All-sky radiance data	MHS	MHS and ATMS
Observation operator	RTTOV v11.3	RTTOV v13.0
Observation error	Inflated by twice the standard deviation of O-B	Geer and Bauer (2011)
O-B check	Constant threshold (10 K)	Different threshold based on cloud amount (30 ~ 37 K)

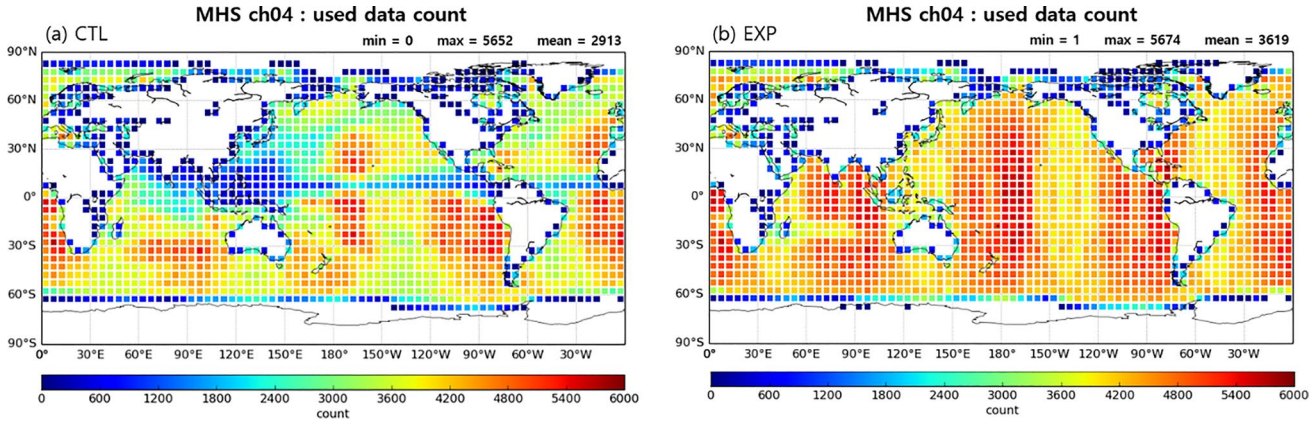

Fig. 1 Accumulated number of observations for MHS channel 4 for (**a**) clear-sky assimilation (CTL); and (**b**) all-sky assimilation (EXP) during the cycling period

assimilation were used as constant values. We chose the root-mean-square errors (RMSEs) of the analysis and forecast from the synchronistic ECMWF Integrated Forecasting System (IFS) analysis data from a 0.25° latitude-longitude grid to measure the quality of the assimilated all-sky radiance data. The IFS model consists of the state-of-the-art data assimilation system, on which the ERA5 is made based, and its superiority was shown in a comparison of forecast skill using the same numerical model and the different initial conditions (Hersbach

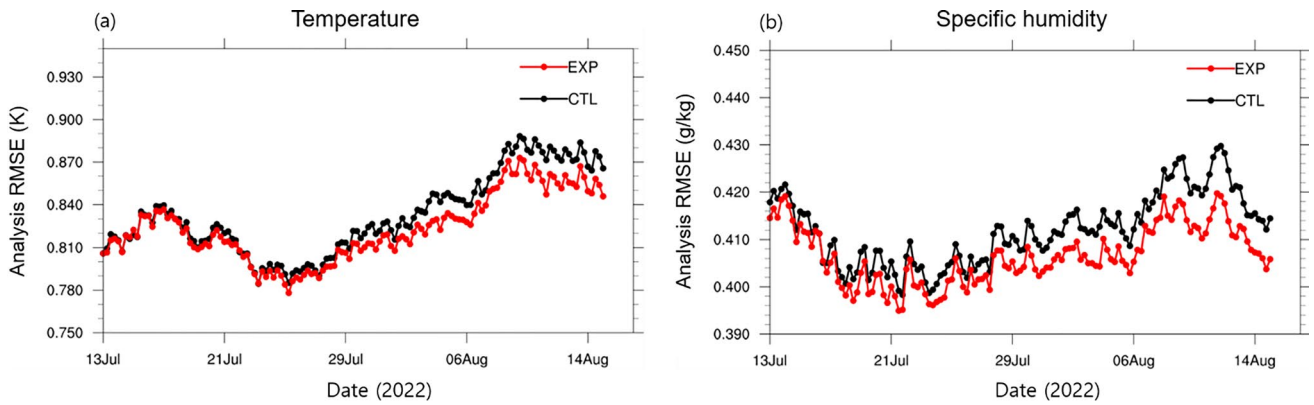

Fig. 2 (**a**) Timeseries of global-averaged root-mean-square-error (RMSE) for temperature (unit: K) and (**b**) specific humidity (unit: g·kg^{-1}) against IFS analysis from July 13, 2022, to August 15, 2022, for 6-hour interval analysis-forecast cycles of the hybrid 4D-EnVar system

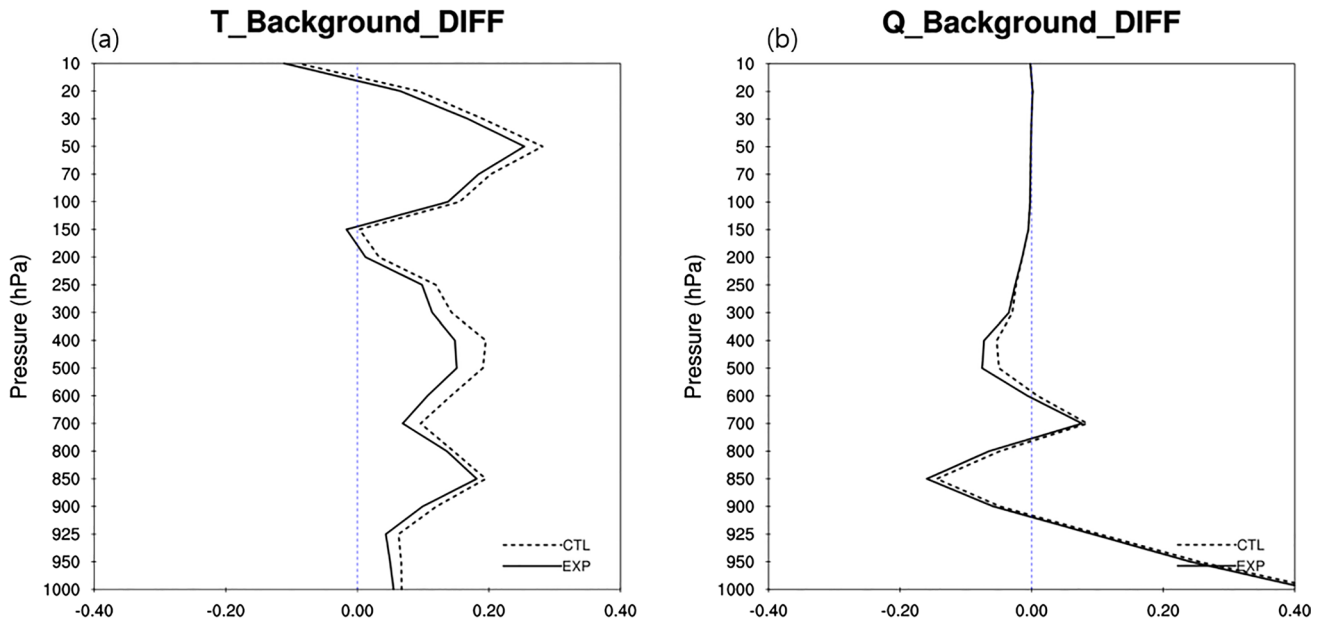

Fig. 3 (**a**) Vertical difference of global-averaged temperature (unit: K) and (**b**) specific humidity (unit: g·kg^{-1}) against IFS analysis for the cycling period

et al. 2020; López-Reyes et al. 2023). A previous study on KIM's all-sky radiance assimilation is introduced in detail by Lee et al. (2020). The discrepancies between the current study and Lee et al. (2020) are presented in Table 1.

Figure 1 shows all available MHS observations for clear-sky assimilation (CTL) and all-sky assimilation (EXP) sampled only over the ocean. Compared to CTL, an approximate 9 ~ 20% more observations were assimilated using the all-sky approach. Although CTL loses many observations throughout East Asia and tropical regions (Fig. 1a), EXP provides uniform coverage over most of the globe (Fig. 1b). We expected that consistency in the coverage of radiance data over East Asia would increase the persistence of the accuracy of precipitation forecasts.

3 Results

3.1 Global Analysis Impact for All-sky Radiance Assimilation

Improvements in the temperature and humidity analyses directly affected by the all-sky radiance assimilation is remarkable (Fig. 2). It can be observed that the difference in the analysis performance between CTL and EXP increases in the later part of the cycle. The beneficial impact of all-sky radiance assimilation is also seen in the improvement of the temperature background throughout the model layer (Fig. 3a). Unfortunately, the bias in specific humidity shows little improvement (Fig. 3b). The humidity bias was similar in the lower troposphere; however, the dry bias

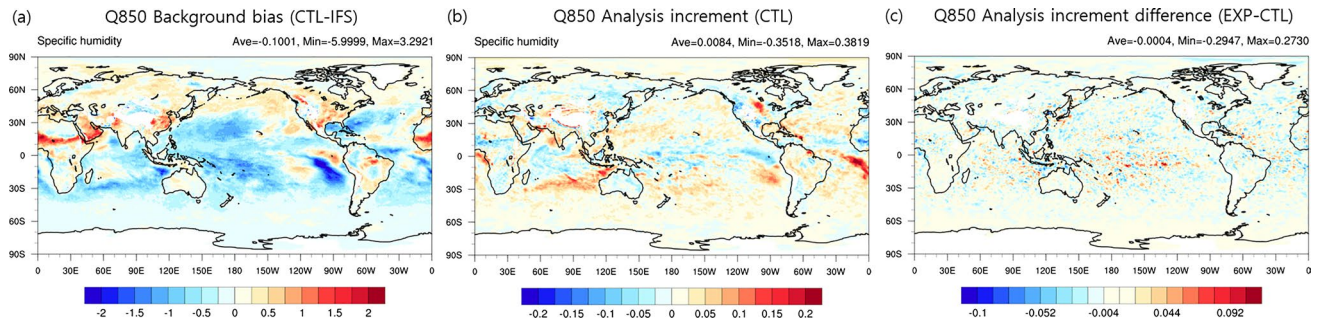

Fig. 4 Spatial distributions of specific humidity (unit: g·kg^{-1}) at 850 hPa: (**a**) background bias for CTL, (**b**) analysis increment for CTL, and (**c**) analysis increment difference between CTL and EXP during the cycling period

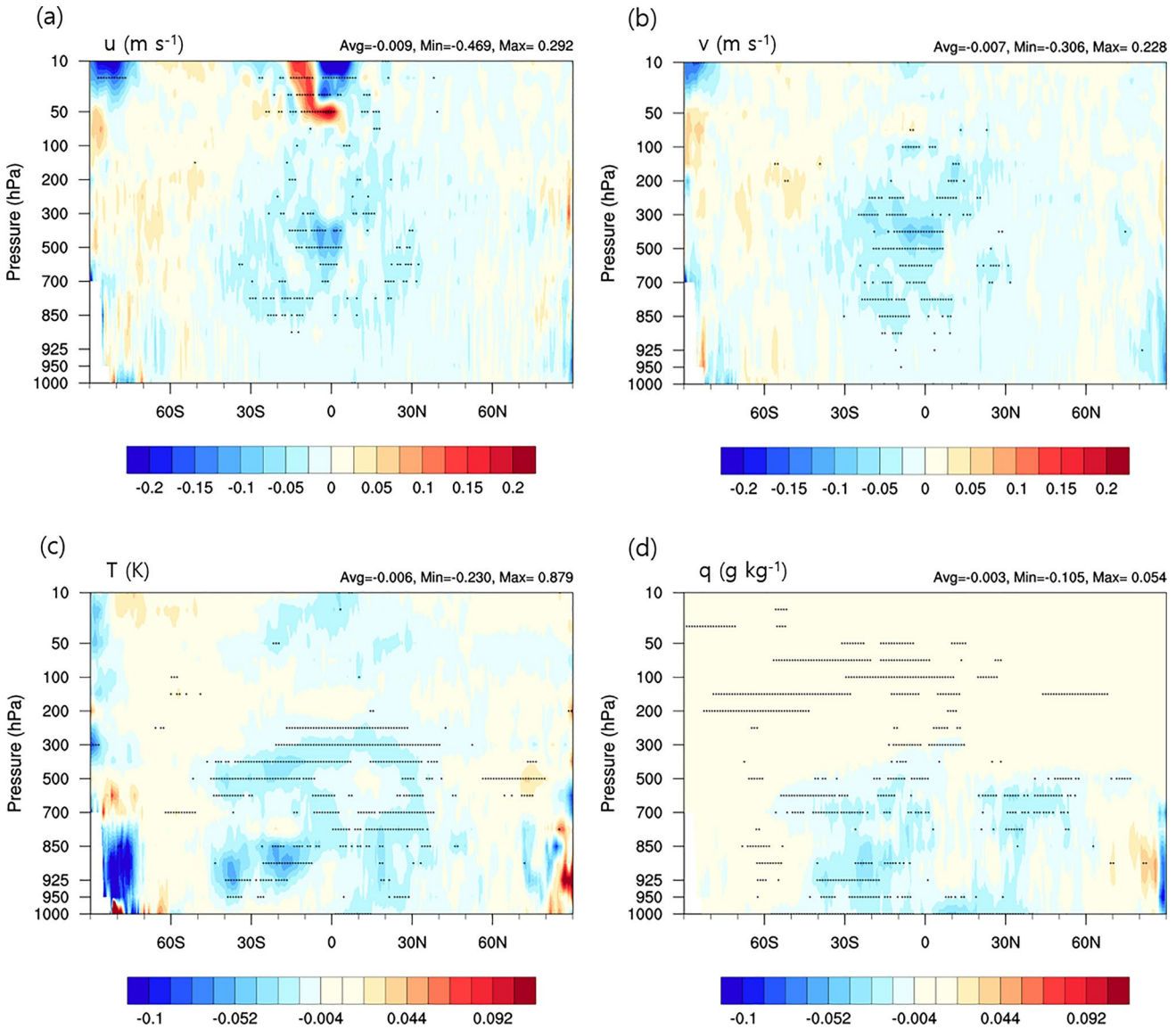

Fig. 5 Composite of the analysis error reductions for (**a**) zonal wind ($m \cdot s^{-1}$), (**b**) meridional wind ($m \cdot s^{-1}$), (**c**) temperature (K), and (**d**) specific humidity ($g \cdot kg^{-1}$) against IFS analysis from July 13, 2022, to August 15, 2022, for 6-hour interval analysis-forecast cycles of the hybrid 4D-EnVar system. Blue and red shading denote beneficial and negative analysis impacts of the EXP, respectively. The small black dots indicate a 95% significant difference, verified by a *t*-test, between the CTL and EXP.

increased slightly at approximately 500 hPa. This is because the moisture is fluent below 925 hPa; wet bias of the KIM is dominant there; the dry analysis increment induced from the lower level that corrected the wet bias at the lower level tends to corrupt the wet bias at the upper level.

Meanwhile, the dry bias of the KIM is dominant at 850 hPa. As seen in Fig. 4a, the one-month averaged bias in specific humidity is negative (-0.1001 $g \cdot kg^{-1}$) which covers the tropics and the southern hemisphere. Although the negative bias in the tropics worsens slightly in clear-sky radiance assimilation (Fig. 4b), in the all-sky assimilation, the difference in analysis increments corrects the worsening bias of the CTL analysis increment in the tropics (Fig. 4c).

Even if observations are sensitive to a particular model variable, if continued in cycles, the effect often spreads to other variables (Lee and Song 2018). It was confirmed that the assimilation of all-sky radiation in this study also affected temperature and wind parameters. Figure 5 shows the zonal average of the analysis (0-hour forecast) error reduction of the zonal wind (-0.7%), meridional wind (-0.6%), temperature (-1.1%) and specific humidity (-1.3%) from 0000 UTC on 13 July to 1800 UTC on 15 August, 2022, excluding a spin-up period. The beneficial wind

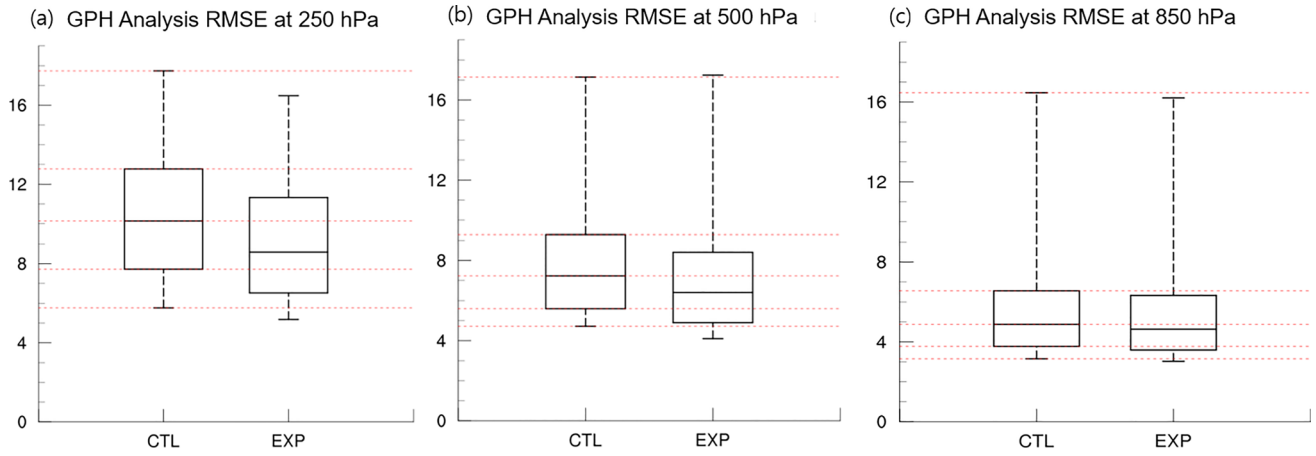

Fig. 6 Box plots of global-averaged analysis RMSE for GPH (unit: m) at (**a**) 250 hPa, (**b**) 500 hPa, and (**c**) 850 hPa against IFS analysis from July 13, 2022, to August 15, 2022

analysis impact of all-sky radiance assimilation was significant in the tropics, around 30˚S–30˚N for 100–850 hPa (Fig. 5a and b). Although the beneficial impact on the wind component focuses on tropical regions, a remarkably substantial positive impact on the mass components (e.g., temperature and specific humidity) expands around the subtropical region and the Northern Hemisphere mid-latitudes for the lower tropospheric levels (Fig. 5c and d).

In both experiments, the background quality of the mass variable is linked to the GPH performance. Figure 6 shows the GPH analysis errors at different model levels. The improvement in GPH in the upper atmosphere (250 hPa) is relatively larger than that in the lower atmosphere (850 hPa). At 500 hPa, the RMSE of GPH-500 hPa for EXP is smaller than that for CTL (Fig. 6b). The analysis performance of the mass variables (i.e., the initial conditions of the KIM) will affect the performance of the model forecast. This motivated us to study the weather forecast performance of extremely heavy rainfall on 9 August 2022, the mechanism of which has been examined by Oh et al. (2023) for all-sky radiance assimilation.

3.2 Case Study of the Precipitation Event

On August 9, 2022, the precipitation system was located within a narrow east-to-west band, with variations in rainfall amounts across the Korean Peninsula (Fig. 7). From the pressure system centering in Mongolia, the pressure trough

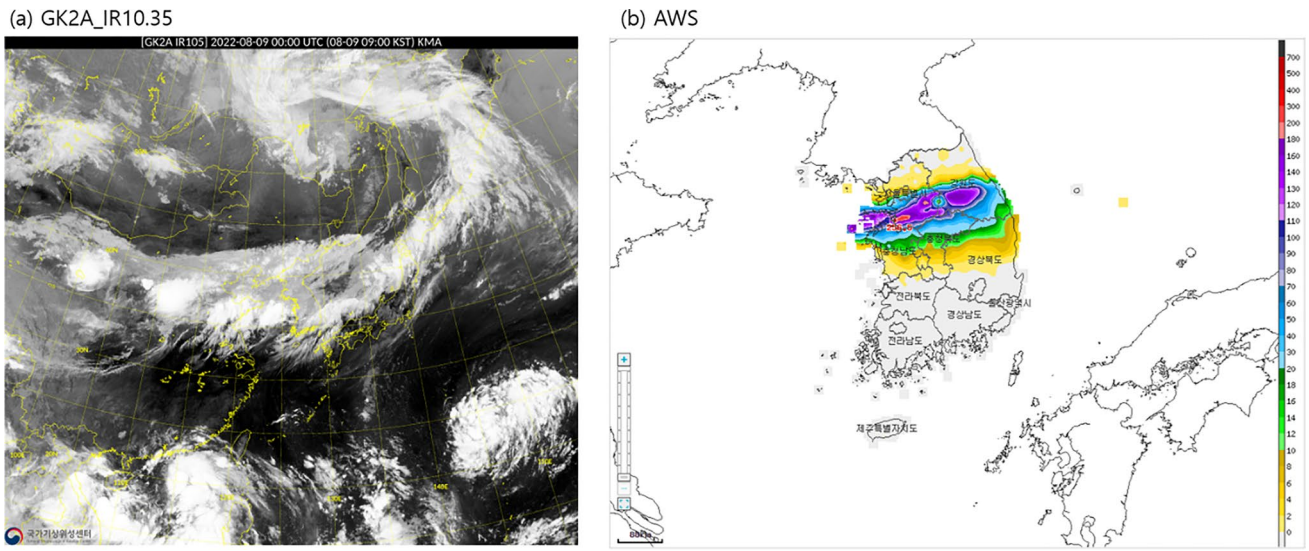

Fig. 7 (**a**) Geo-KOMPSAT 2 A (GK2A) IR channel (10.35 μm) image; and (**b**) 24-hour accumulated rainfall amount (in mm) from the Automatic Weather Systems (AWS) observations at 0000 UTC on August 9, 2022

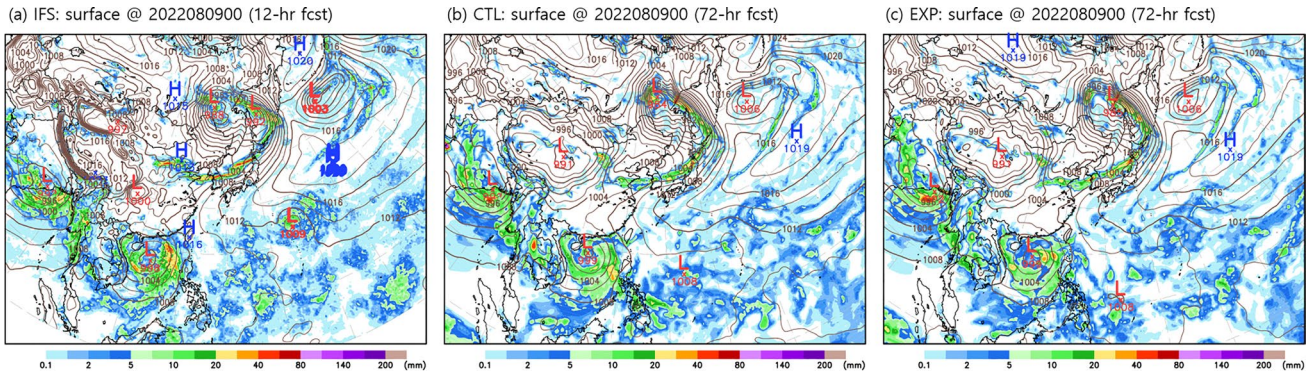

Fig. 8 (**a**) ECMWF's IFS weather chart with a 12-hour forecast; (**b**) the KIM's 72-hour forecast weather charts from CTL; and (**c**) EXP at the surface, at 0000 UTC on August 9, 2022. The solid line represents sea level pressure (hPa), and the color shading represents the 6-hour accumulated precipitation (mm)

stretching its assembly in the southwest direction will take the form of connecting a line in the west direction with a strong pressure trough in a row from the Chinese mainland (Fig. 8).

The main elements of this synoptic pattern were simulated differently according to the initial conditions, even when using the same numerical forecasting model was used (Fig. 8). In Fig. 8, the first panel shows the IFS of the ECMWF 12-hour forecast field used as a reference, and the center and right panels are the 72-hour forecast field for August 9, 2022, at 0000 UTC predicted in the clear-sky and all-sky experiments, respectively. As shown in Fig. S1 (a different version of Fig. 8 focused on the Korean Peninsula), the precipitation cores over Korea and northern Japan are stronger in EXP rather than in CTL to be more similar to those in the reference field from the IFS. Oh et al. (2023) explained the dynamic components represented by wind were the main cause of this rainfall event, with a subsequent aid, approximately 30% of the total contributions of the thermodynamic component represented by the moisture content. Based on this examination, the differences in the precipitation systems simulated in clear-sky and all-sky experiments were investigated.

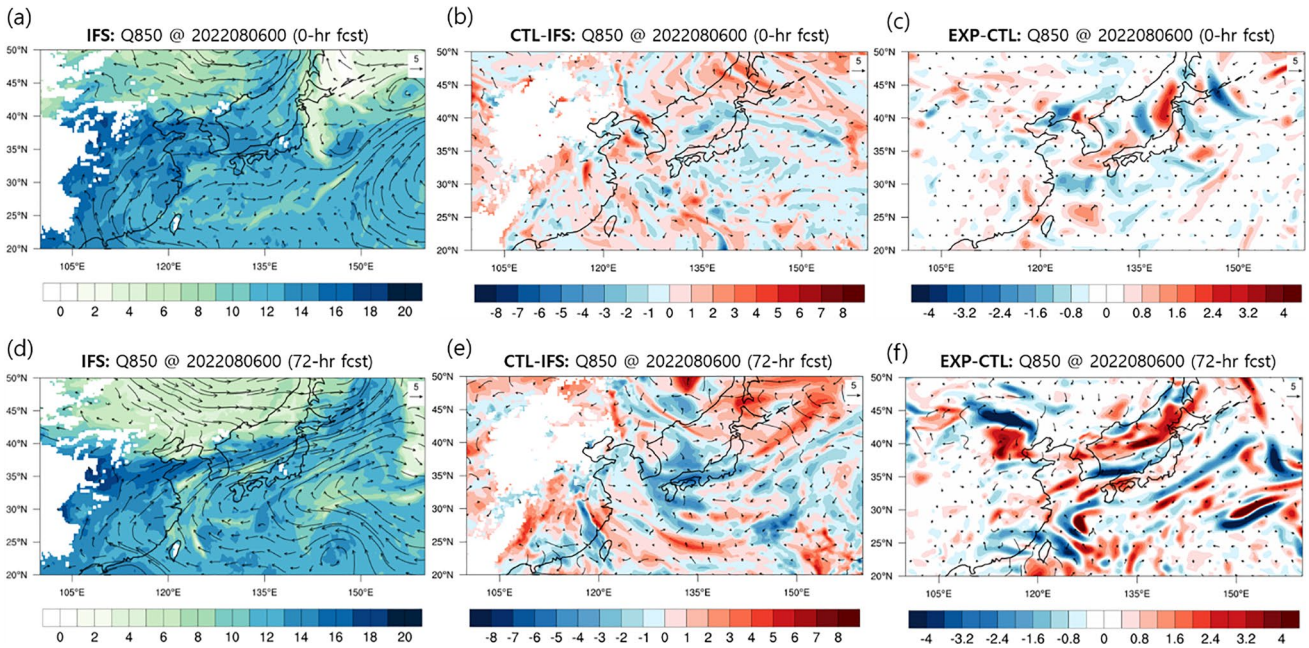

Fig. 9 Fields of 850 hPa-specific humidity ($g \cdot kg^{-1}$) and 850 hPa-wind vector ($m \cdot s^{-1}$) at KIM's initial (upper) and 72-hour forecast (lower): IFS (**a**, **c**), the difference between CTL and IFS (**b**, **e**) and the difference between EXP and CTL (**c**, **f**). The initial time is 0000 UTC on August 6, 2022, and the forecast target time is 0000 UTC on August 9, 2022

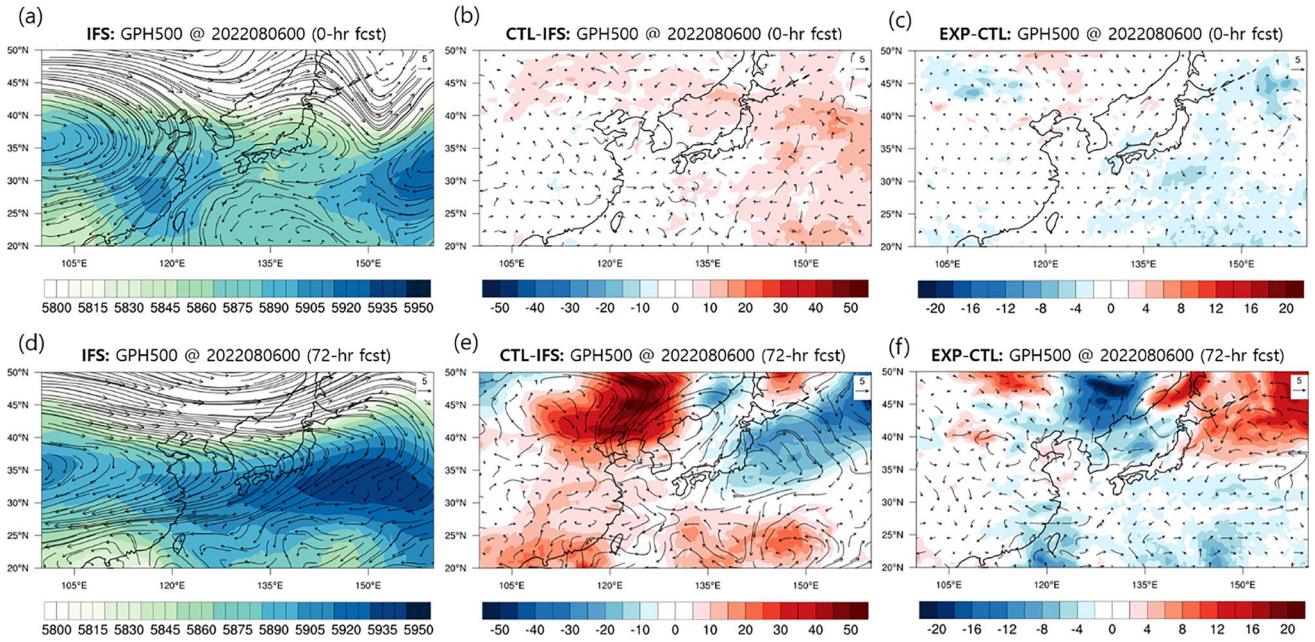

Fig. 10 Fields of 500 hPa-GPH (unit: m) and 200 hPa-wind vector ($m \cdot s^{-1}$) at KIM's initial (upper) and 72-hour forecast (lower): IFS (**a**, **c**), the difference between CTL and IFS (**b**, **e**) and the difference between EXP and CTL (**c**, **f**). The initial time is 0000 UTC on August 6, 2022, and the forecast target time is 0000 UTC on August 9, 2022

In both experiments, differences in specific humidity and winds at 850 hPa were not apparent (Fig. 9). Nevertheless, we note that the overestimation of humidity in the initial condition of the CTL, with a domain-averaged bias of $+0.061$ $g \cdot kg^{-1}$ (Fig. 9b), becomes smaller in the EXP with all-sky radiance assimilation, with a domain average of -0.026 $g \cdot kg^{-1}$. (Fig. 9c). This is consistent with the results of the all-sky radiance experiment of making the humidity field drier, as shown in Fig. 3b.

The western North Pacific subtropical high (WNPSH) stretched abnormally north to near Japan on August 9, 2022 (refer to Fig. 5 in Oh et al. 2023), which was designated as the main cause of this record-breaking rainfall event, creating a strong frontal conflict in the air over land and ocean in this monsoon season. The all-sky radiance assimilation improved the quality of the analysis of the overall levels of GPH, as shown in Fig. 6 and S2. The WNPSH is mainly expressed as a 500 hPa GPH. In the clear-sky assimilation experiment, the northward movement of the WNPSH was blocked, with an underestimation of the 500-hPa GPH over the ocean east of Japan (Fig. 10e). This underestimation was

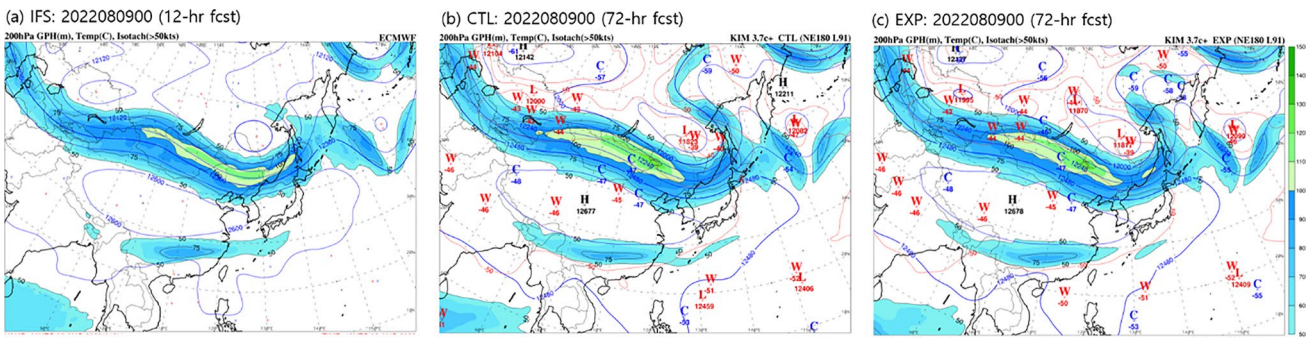

Fig. 11 Comparison of the horizontal wind speed (colored shading; $m \cdot s^{-1}$), GPH (solid contours; m) and temperature (dashed contours; °C) at 200 hPa, from (**a**) ECMWF's IFS weather chart with a 12-hour forecast, (**b**) KIM 72-hour forecast weather charts of CTL and (**c**) EXP. Centers of high (H) and low (L) pressure, and warm (W) and cold (C) air, are marked with bold letters. The target time is 0000 UTC on August 9, 2022

countered in the all-sky radiance assimilation experiment with a feature closer to the IFS GPH (Fig. 10f).

The upper troposphere above the northern part of the Korean Peninsula passed through the jet stream (Figs. 10d and 11a). There is an upper-level convergence zone to the right south of the exit of the jet stream (Holton 2004). In the reference field of 12-hour forecast of the IFS targeting August 9, 2022, the exit of the jet stream is not located over the north of the Korean Peninsula. However, the low-pressure difference in the 72-hour forecast of the CTL experiment (Fig. 10e) contributes to changing the northeastern region of the Korean Peninsula to the exit of the jet stream (Fig. 11b). In the all-sky experiment, the low-pressure anomaly was restricted by high-pressure wind flow to extend the range of the jet stream.

4 Summary and Implications

This paper presents the results of the recent development of the all-sky radiance assimilation system in the KIM. The experimental period covered the record-breaking heavy rainfall event on August 9, 2022. Improvements in the humidity field in the all-sky experiment were transferred to the temperature, GPH, and wind fields.

Oh et al. (2023) examined the dynamic and thermodynamic causes of the rainfall event. Based on their analysis, the WNPSH is a crucial factor for that event, and we examined the accuracy of the simulation of the WNPSH in clear-sky and all-sky experiments. In the clear-sky experiment, northward propagation of the WNPSH was restricted, and a humid bias exists with clear-sky radiance assimilation over the WNPSH region. Humid air is lighter than dry air; therefore, the GPH should be lower to achieve the same pressure, and a low-pressure bias occurs. All-sky radiance assimilation makes the moisture field drier, which helps elevate the GPH over the WNPSH region. The expansion of the WNPSH yielded a steeper confrontation in the air between land and ocean around the southeastern sea of the Korean Peninsula. A more accurate simulation of the jet stream outlet was also demonstrated in an all-sky experiment. This study shows that the all-sky radiance assimilation can help to more accurately predict extreme rainfall events through proper simulations of large-scale fields.

The variation in the jet stream outlet is also shown according to the different methods of assimilating the radiance data. In the future, it is expected that an analysis with more statistical significance tests will be possible through correlation analysis using ensemble initial conditions.

Several future research items remain in the area of all-sky radiance data assimilation, including the solution to the mismatch in cloud areas between the model and observation, bias correction of all-sky radiance observations, and modeling of observation error covariance (Okamoto et al. 2023). The application of new approaches, such as artificial intelligence to these issues, is a prospective subject of research.

Supplementary Information The online version contains supplementary material available at https://doi.org/10.1007/s13143-024-00365-5.

Acknowledgements This work was carried out through the R&D project "Development of a Next-Generation Data Assimilation System by the Korea Institute of Atmospheric Prediction Systems (KIAPS)", funded by the Korea Meteorological Administration (KMA2020-02211) and the Korea Environment Industry & Technology Institute (KEITI) through the "Climate Change R&D Project for New Climate Regime", funded by the Korea Ministry of Environment (MOE) (2022003560006).

Declarations

Conflict of interest The authors have no conflicts of interest to declare.

References

Argence, S., Lambert, D., Richard, E., Chaboureau, J.P., Söhne, N.: Impact of initial condition uncertainties on the predictability of heavy rainfall in the Mediterranean: A case study. Q. J. R. Meteorol. Soc. **134**(636), 1775–1788 (2008)

Bae, S.Y., Hong, S.-Y., Lim, K.-S.: Coupling WRF double-moment 6-class microphysics schemes to RRTMG radiation scheme in weather research forecasting model. Adv. Meteorol. **2016.** (2016). https://doi.org/10.1155/2016/5070154

Baek, S.H.: A revised radiation package of G-packed McICA and two-stream approximation: Performance evaluation in a global weather forecasting model. J. Adv. Model. Earth Syst. **9**, 1628–1640 (2017). https://doi.org/10.1002/2017MS000994

Bauer, P., Moreau, E., Chevallier, F., O'Keeffe, U.: Multiple-scattering microwave radiative transfer for data assimilation applications. Q. J. R. Meteorol. Soc. **132**, 1259–1281 (2006)

Bloom, S.C., Takacs, L.L., da Silva, A.M., Ledvina, D.: Data assimilation using incremental analysis updates. Mon. Weather Rev. **124**(4), 1256–1271 (1996)

Choi, H.-J., Hong, S.-Y.: An updated subgrid orographic parameterization for global atmospheric forecast. J. Geophys. Res. Atmos. **120**, 12445–12457 (2015). https://doi.org/10.1002/2015JD024230

Choi, S.J., Hong, S.-Y.: A global non-hydrostatic dynamical core using the spectral element method on a cubed-sphere grid. Asia-Pac. J. Atmos. Sci. **52**, 291–307 (2016)

Eriksson, P., Ekelund, R., Mendrok, J., Brath, M., Lemke, O., Buehler, S.A.: A general database of hydrometeor single scattering properties at microwave and submillimeter wavelengths. Earth

Syst. Sci. Data **10**, 1301–1326 (2018). https://doi.org/10.5194/essd-10-1301-2018

Geer, A.J., Baordo, F., Bormann, N., Chambon, P., English, S.J., Kazumori, M., Lawrence, H., Lean, P., Lonitz, K., Lupu, C.: The growing impact of satellite observations sensitive to humidity, cloud and precipitation. Q. J. R. Meteorol. Soc. **143**, 3189–3206 (2017)

Geer, A.J., Baordo, F., Bormann, N., English, S.: All-sky assimilation of Microwave Humidity sounders. ECMWF Tech. Memorandum **741**, 1–57 (2014). https://doi.org/10.21957/obosmx154

Geer, A.J., Bauer, P.: Observation errors in all-sky data assimilation. Q. J. R. Meteorol. Soc. **137**, 2024–2037 (2011)

Geer, A.J., Bauer, P., Lonitz, K., Barlakas, V., Eriksson, P., Mendrok, J., Doherty, A., Hocking, J., Chambon, P.: Bulk hydrometeor optical properties for microwave and sub-millimetre radiative transfer in RTTOV-SCATT v13.0. Geosci. Model. Dev. **14**, 7497–7526 (2021)

Geer, A.J., Lonitz, K., Weston, P., Kazumori, M., Okamoto, K., Zhu, Y., Liu, E.H., Collard, A., Bell, W., Migliorini, S., Chambon, P., Fourrie, N., Kim, M.J., Kopken–Watts, C., Schraff, C.: All-sky satellite data assimilation at operational weather forecasting centres. Q. J. R. Meteorol. Soc. **144**, 1191–1217 (2018)

Han, J.-Y., Hong, S.-Y., Lim, K.-S.S., Han, J.: Sensitivity of a cumulus parameterization scheme to precipitation production representation and its impact on a heavy rain event over Korea. Mon. Wea Rev. **144**, 2125–2135 (2016)

Hersbach, H., Bell, B., Berrisford, P., Hirahara, S., Horányi, A., Muñoz-Sabater, J., Nicolas, J., Peubey, C., Radu, R., Schepers, D., Simmons, A., Soci, C., Abdalla, S., Abellan, X., Balsamo, G., Bechtold, P., Biavati, G., Bidlot, J., Bonavita, M., De Chiara, G., Dahlgren, P., Dee, D., Diamantakis, M., Dragani, R., Flemming, J., Forbes, R., Fuentes, M., Geer, A., Haimberger, L., Healy, S., Hogan, R.J., Hólm, E., Janisková, M., Keeley, S., Laloyaux, P., Lopez, P., Lupu, C., Radnoti, G., de Rosnay, P., Rozum, I., Vamborg, F., Villaume, S., Thépaut, J.-N.: The ERA5 global reanalysis. Q. J. R. Meteorol. Soc. **146**, 1999–2049 (2020)

Holton, J.R.: An Introduction to Dynamic Meteorology. Academic Press, Massachusetts (2004)

Hong, S.-Y., Dudhia, J., Chen, S.-H.: A revised approach to ice microphysical processes for the bulk parameterization of clouds and precipitation. Mon. Wea. Rev. **132**(1), 103–120 (2004)

Hong, S.Y., Kwon, Y.C., Kim, T.-H., Kim, J.-E., Choi, S.-J., Kwon, I.-H., Kim, J., Lee, E.-H., Park, R.-S., Kim, D.-I.: The Korean Integrated Model (KIM) system for global weather forecasting. Asia-Pac. J. Atmos. Sci. **54**(1), 267–292 (2018)

Kang, J.-H., Chun, H.-W., Lee, S., Ha, J.-H., Song, H.-J., Kwon, I.-H., Han, H.-J., Jeong, H., Kwon, H.-N., Kim, T.-H.: Development of an observation processing package for data assimilation in KIAPS. Asia-Pac. J. Atmos. Sci. **54**(1), 303–318 (2018)

Khadke, L., Pattnaik, S.: Impact of initial conditions and cloud parameterization on the heavy rainfall event of Kerala Model (2018). Earth Syst. Environ. **7**, 2809–2822 (2021)

Koo, M.-S., Baek, S., Seol, K.-H., Cho, K.: Advances in land surface modeling of KIAPS based on the Noah land surface model. Asia-Pac. J. Atmos. Sci. **53**(3), 361–373 (2017). https://doi.org/10.1007/s13143-017-0043-2

Kwon, Y.C., Hong, S.-Y.: A mass-flux cumulus parameterization scheme across gray-zone resolutions. Mon. Wea. Rev. 583–598 (2017). https://doi.org/10.1175/MWR-D-16-0034.1

Kwon, I.-H., Song, H.-J., Ha, J.-H., Chun, H.-W., Kang, J.-H., Lee, S., Lim, S., Jo, Y., Han, H.-J., Jeong, H., Kwon, H.-N., Shin, S., Kim, T.-H.: Development of an operational hybrid data assimilation system at KIAPS. Asia-Pac. J. Atmos. Sci. **54**(1), 319–335 (2018)

Lee, E.-H., Lee, E., Park, R., Kwon, Y.C., Hong, S.-Y.: Impact of turbulent mixing in the Stratocumulus-Topped Boundary Layer on Numerical Weather Prediction. Asia-Pac. J. Atmos. Sci. **54**(s), 371–384 (2018). https://doi.org/10.1007/s13143-018-0024-0

Lee, S., Song, H.J.: Impacts of LEOGEO Atmospheric Motion vectors on east Asian weather forecasts. Q. J. R. Meteorol. Soc. **144**(715), 1914–1925 (2018)

Lee, S., Song, H.J., Chun, H.W., Kwon, I.H., Kang, J.H., Lim, S.: All-sky microwave humidity sounder assimilation in the Korean Integrated Model forecast system. Q. J. R. Meteorol. Soc. **146**(732), 3570–3586 (2020)

Lee, S., Song, H.-J., Kwon, I.-H., Kang, J.-H.: Impacts of Aeolus horizontal Line-Of-Sight (HLOS) wind assimilation on the Korean integrated model (KIM). Atmos. Sci. Lett. **24**, e1138 (2022). https://doi.org/10.1002/asl.1138M

López-Reyes, M., Gónzalez-Alemán, J.J., Sastre, M., Insua-Costa, D., Bolgiani, P., Martín, M.L.: On the impact of initial conditions in the forecast of Hurricane Leslie extratropical transition. Atmos. Res. **295**, 107020 (2023). https://doi.org/10.1016/j.atmosres.2023.107020

Oh, H., Ha, K.J., Jeong, J.Y.: Identifying dynamic and thermodynamic contributions to the record-breaking 2022 summer Extreme Rainfall events in Korea. Asia-Pac J. Atmos. Sci. 1–13 (2023). https://doi.org/10.1007/s13143-023-00334-4

Okamoto, K., Ishibashi, T., Okabe, I.: All-sky infrared radiance assimilation of a geostationary satellite in the Japan Meteorological Agency's global system. Q. J. R. Meteorol. Soc. **149**(755), 2477–2503 (2023)

Okamoto, K., Sawada, Y., Kunii, M.: Comparison of assimilating all-sky and clear-sky infrared radiances from Himawari-8 in a mesoscale system. Q. J. R. Meteorol. Soc. **145**, 745–766 (2018)

Park, R.-S., Chae, J.-H., Hong, S.-Y.: A revised prognostic cloud fraction scheme in a global forecasting system. Mon. Wea. Rev. **114**, 1219–1229 (2016). https://doi.org/10.1175/MWR-D-15-0273.1

Shin, S., Kang, J.-H., Chun, H.-W., Lee, S., Sung, K., Cho, K., Jo, Y., Kim, J.-E., Kwon, I.-H., Lim, S., Kang, J.-S.: Real data assimilation using the local ensemble transform Kalman Filter (LETKF) system for a global non-hydrostatic NWP model on the cubed-sphere. Asia-Pac. J. Atmos. Sci. **54**, 351–360 (2018)

Song, H.-J., Kwun, J., Kwon, I.-H., Ha, J.-H., Kang, J.-H., Lee, S., Chun, H.-W., Lim, S.: The impact of the nonlinear balance equation on a 3D-Var cycle during an australian-winter month as compared with the regressed wind–mass balance. Q. J. R. Meteorol. Soc. **143**, 2036–2049 (2017)